

## THE IMPACT OF HD COOLING ON THE FORMATION OF THE FIRST STARS

IAN D. MCGREER AND GREG L. BRYAN

Department of Astronomy, Columbia University, Pupin Physics Laboratories, New York, NY 10027  
*Draft version November 7, 2018*

### ABSTRACT

We use numerical simulations to investigate the importance of HD formation and cooling on the first generation of metal-free stars in a  $\Lambda$ CDM cosmology. We have implemented and tested non-equilibrium HD chemistry in an adaptive mesh refinement simulation code and applied it to two situations. (1) It is first applied to the formation of  $10^5 - 10^6 M_{\odot}$  halos which form in the absence of any ionizing source (“unperturbed” halos). We show, in agreement with previous work, that HD cooling is of only marginal importance for most halos; however, we find that for the lowest mass halos, with masses a few times  $10^5 M_{\odot}$ , HD cooling can equal or surpass the  $H_2$  cooling rate. This leads to a population of stars formed in halos with effective HD cooling that are less massive by a factor of  $\sim 6$  compared to halos dominated by  $H_2$  cooling. (2) In the second part of the paper, we ionize the halos in order to explore the impact of HD cooling in the presence of an ample population of free electrons. This leads to cooler temperatures (due to the electron-catalyzed production of  $H_2$ ) implying somewhat lower resulting proto-stellar mass. Adding HD chemistry changes this by lowering the temperature further, to the level of the CMB. We find that HD cooling dominates over  $H_2$  cooling in the density range  $10^2 \text{ cm}^{-3}$  to  $10^6 \text{ cm}^{-3}$ , but above this density, the temperature rises and  $H_2$  cooling dominates again. Because of this, the accretion rate on to the protostar is almost the same as in the  $H_2$  case (at least for accreted masses below  $50\text{-}100 M_{\odot}$ ), therefore we argue that HD cooling in ionized halos will probably not result in a population of significantly lower mass stars.

*Subject headings:* cosmology:theory – galaxies: high-redshift – galaxies:formation – stars:formation – methods: N-body simulations

### 1. INTRODUCTION

The conditions surrounding the formation of the first stars out of primordial gas has been the focus of much work over the last few years, and has recently been summarized by Bromm & Larson (2004) and Ciardi & Ferrara (2005). The picture that emerges is that of the first stars forming in halos with masses around  $10^6 M_{\odot}$  due to cooling from molecular hydrogen (e.g., Couchman & Rees 1986; Haiman et al. 1996; Tegmark et al. 1997; Abel et al. 2002; Yoshida et al. 2003). The actual masses of the first stars are less well determined, but in the last five years a number of groups have employed high-resolution hydrodynamic simulations, using both adaptive Eulerian codes (e.g., Abel et al. 2002; O’Shea & Norman 2007) and smoothed particle hydrodynamics (SPH) Lagrangian codes (e.g., Bromm et al. 2002; Yoshida et al. 2003, 2006; Gao et al. 2007) to answer this question. This work has generally resulted in the formation of a single, relatively high mass (of order  $100 M_{\odot}$ ) star forming in each halo. The resulting ionization front from the first star ionizes the original cloud before any other stars can form (Whalen et al. 2004; Kitayama et al. 2004; Abel et al. 2007).

Much of the early work focused on single objects that formed within the most massive halo in the simulation volume. More recently, some groups have explored the parameter space by conducting multiple simulations with different initial conditions and box sizes (O’Shea & Norman 2007) and with varying cosmological parameters (Gao et al. 2007). In general, a fairly consistent picture results: massive stars form in overdense regions (halo masses  $\sim 10^6 M_{\odot}$ ) less than a billion years

after the big bang ( $10 \lesssim z \lesssim 30$ ).

Most first star simulations have relied on a nine species chemical reaction network consisting of hydrogen, helium, molecular hydrogen, and their associated ions (e.g., Abel et al. 1997). This simple model is possible because big bang nucleosynthesis produced only lithium and lighter elements. While only trace amounts of  $H_2$  are present initially within the primordial gas, it forms rapidly in the high density gas within collapsing halos, and once the density exceeds  $n \sim 10^8 \text{ cm}^{-3}$  the three-body formation process drives the fraction of molecular hydrogen to near unity.

$H_2$  has been shown to be effective in cooling primordial gas within dense halos, lowering the gas temperature to  $\sim 200\text{K}$ . However, the  $H_2$  molecule itself is a relatively poor coolant since it lacks a permanent electric dipole moment. On the other hand, the HD molecule has a permanent dipole, and cools more effectively at low temperatures ( $\lesssim 200\text{K}$ ). This has led several authors to suggest that HD will have an important effect on first star formation (Puy et al. 1993; Galli & Palla 1998; Stancil et al. 1998).

However, in low-mass primordial halos, the temperature never falls below about  $200\text{K}$ , which is required for HD to dominate over  $H_2$  cooling, and so the general consensus has been that HD is unimportant for primordial, low-mass halos. For example, Bromm et al. (2002) included HD chemistry in 3D SPH simulations of first star formation and found that  $H_2$  cooling dominated; Yoshida et al. (2006) came to the same conclusion. Ripamonti (2007) recently conducted a suite of 1D simulations with full HD chemistry and found that for typical halos this is true, but that in low mass halos

( $\lesssim 3 \times 10^5 M_\odot$ ) HD is formed in sufficient quantities to be as important in cooling the gas as  $H_2$ . In one run, HD cooling lowered the temperature of the gas to  $\sim 70K$ , 3-4 times lower than when HD was neglected. Ripamonti (2007) argued that the Jeans mass in such halos is lowered by a factor of 10, implying that significantly lower mass stars will form in these regions. This is an intriguing suggestion and one of the motivations of this paper is to test this idea using full three-dimensional simulations.

While there is general (but not universal) agreement that HD is likely to be mostly unimportant in low-mass halos that have never been ionized, a number of authors have recently pointed out that HD will form in high abundance when the gas is ionized (as originally pointed out by Shapiro & Kang 1987). For example, Nagakura & Omukai (2005) used one-dimensional models to follow the evolution of HII regions inside massive halos. They found that for high enough masses, the gas would re-collapse and form significant amounts of HD due to the presence of free electrons. This cooling lowered the gas temperature to the CMB temperature and so the authors suggested that low mass stars (of order  $1 M_\odot$ ) could result. Machida et al. (2005) also looked at the impact of HD cooling in the swept up shells of primordial supernovae (see also Salvaterra et al. 2004).

More generally, Johnson & Bromm (2006) used one zone models to show that HD cooling would be important whenever primordial gas was significantly ionized. This included halos forming behind strong shocks, in relic HII regions and in high-mass halos. They showed that the cooling was sufficient to quickly reach the CMB temperature and argued that this would give rise to a Population II.5<sup>1</sup> (Mackey et al. 2003) with masses 10 times lower than traditional Population III stars. Greif & Bromm (2006) went on to suggest that these stars generated the majority of the photons that ionized the universe.

In this paper, we use three-dimensional simulations to explore the impact of HD cooling in two related areas of primordial star formation. The first is to investigate more carefully the role of HD cooling in “unperturbed” low-mass primordial star forming regions, paying particularly close attention to the suggestion of Ripamonti (2007) that HD may play a key role in the lowest mass halos.

In the second part of this paper, we explore the impact that free electrons have on HD cooling in primordial halos. As noted above, ionization can occur for a variety of reasons, including relic HII regions (the kpc-sized regions ionized by nearby primordial stars) and shocks due to mergers with higher mass halos.

We take a deliberately simple approach to the generation of free electrons and we simply ionize and heat the gas instantaneously at a certain point in the evolution of our halos. This is an approximation to more sophisticated models which follow the radiative transfer of the

ionizing radiation and its heating explicitly. Our method is very similar to O’Shea et al. (2005). As discussed more fully in Mesinger et al. (2006), this approach has two distinct differences compared to a more realistic treatment. First, the optically thin radiative cooling approximation means that the dense gas in the core may be improperly ionized (although if the source is in the center of halo itself, this is less of a concern). Second, the instantaneous nature of the heating prevents the gas from being expelled from the halo. The advantage of our approach is that we are able to compare the effect of HD cooling with and without ionization in similar halos, and so we can see the key effects simply and clearly. Also, it is computationally faster and so we can study more cases. Finally, as we will argue later, many of our key results should still apply when carried out with more realistic treatment of the ionization (and indeed, do match other simulations where we can compare).

In the next section, we describe the simulation code and our treatment and tests of HD chemistry. In §3.1, we first examine the impact of HD on primordial halos without ionization, and then in §3.2 we analyze the role of HD cooling in halos with ionization. Section 4 contains a discussion of the general effects of HD cooling in primordial star formation, including predictions for the final masses of stars based on the end state of the simulations. Finally, a brief summary of the results is presented in §5.

## 2. METHODOLOGY

To follow the formation and evolution of the primordial clouds from cosmological initial conditions, we use the Enzo adaptive mesh refinement (AMR) method. It is a well-tested cosmological hydrodynamics scheme that has previously been used to study a number of astrophysical systems including clusters of galaxies (e.g., Bryan & Voit 2001; Younger & Bryan 2007), the ISM (Slyz et al. 2005), the intergalactic medium (Richter et al. 2006), and other applications. In particular, it has been widely used to study the formation of the first stars at high redshift (Abel et al. 2000, 2002; Machacek et al. 2001, 2003; Abel et al. 2007; O’Shea & Norman 2007).

The code is detailed more fully in Bryan & Norman (1997), Bryan (1999), and O’Shea et al. (2004), and so we only summarize it here. The code relies on a hybrid particle-mesh solver (Efsthathiou et al. 1985), using an N-body representation for the collisionless dark matter, and an Eulerian grid for the baryonic component. Enzo includes a second-order accurate piecewise parabolic method solver (Colella & Woodward 1984; Bryan et al. 1995) for solving the hydrodynamic equations. The resolution of the grid is increased over the course of a simulation using the block-structured AMR technique (see Berger & Colella 1989). On every level and at each timestep, the state of the grid is examined to determine if any regions have exceeded critical values in baryonic density, dark matter density, or Jeans length. If so, then the grid is refined in that region by adding more grid points. In this way, the most interesting regions of a collapsing medium receive the highest levels of refinement, and dynamic range large enough to correctly model the small-scale physics of cloud collapse in a cosmologically significant volume is achieved.

As our method and application is very similar to

<sup>1</sup> Stars which formed in primordial, metal-free gas that has been perturbed by a previous generation of stars have often been referred to as Population II.5; i.e., an intermediate generation between Population III and Population II. A recent proposal (O’Shea et al. 2008) is to refer to the “first generation” stars formed in primordial gas as Population III.1, and the “second generation” stars formed in gas of primordial composition but affected by feedback effects from the first generation as Population III.2, a nomenclature we will adopt in this paper.

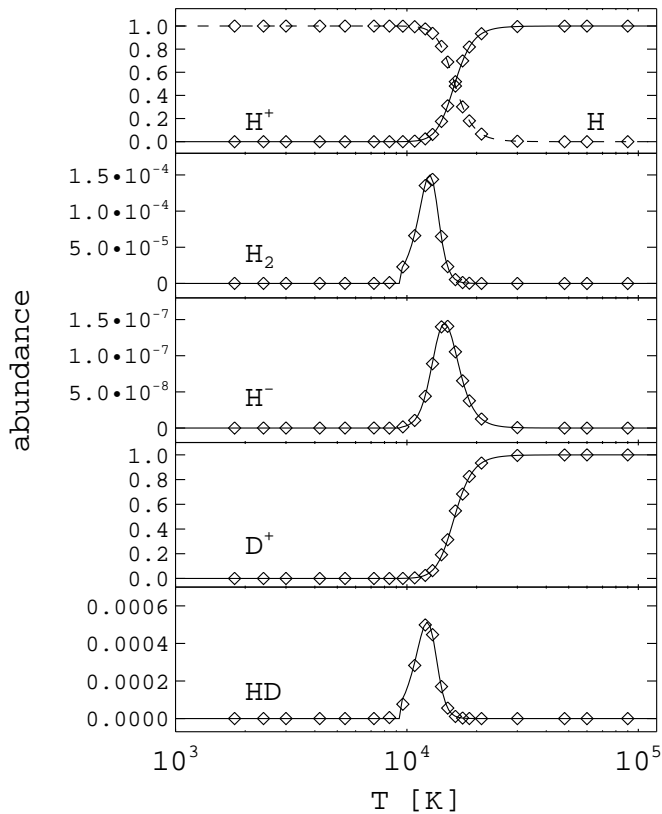


FIG. 1.— Equilibrium abundances of various species obtained from steady-state runs of Enzo. Lines show the analytic expectation from simple derivations based on the reaction rates (see Appendix). Diamond symbols mark the values converged on by adiabatic runs of Enzo (with all radiative cooling turned off), showing that the chemistry solver reproduces the expected values.

Abel et al. (2002) and Machacek et al. (2003), we describe only the changes in detail<sup>2</sup>. In the next two sections, we discuss first our enhanced chemical model and then the details of the simulation setup.

### 2.1. Chemical Model

The first stars formed in a chemically simplified environment consisting of lithium and lighter elements. Cooling from atomic hydrogen and helium is inefficient in the low temperature ( $\lesssim 2000\text{K}$ ) gas within collapsing halos at  $z \sim 20$ , but should enough molecular hydrogen form it can cool the gas to  $T \sim 200\text{K}$ . Abel et al. (1997) and Anninos et al. (1997) developed a chemical model for primordial gas following the evolution of the nine dominant species H,  $\text{H}^+$ ,  $\text{H}^-$ , He,  $\text{He}^+$ ,  $\text{He}^{++}$ ,  $\text{H}_2$ ,  $\text{H}_2^+$ , and  $\text{e}^-$ . Abel et al. (1997) demonstrated that the reaction rates for these species can be reduced to 19 collisional and 9 radiative processes and remain valid over a wide range of temperatures ( $1 < T < 10^8\text{K}$ ) and densities ( $n \lesssim 10^4\text{cm}^{-3}$ ). The rate equations are solved using an implicit scheme based on the backward differencing formula (BDF) technique described in Anninos et al. (1997). Abel et al. (2000) modeled the formation of a primordial molecular cloud using this chemical model,

<sup>2</sup> The code used is nearly identical to the public version of Enzo described in O’Shea et al. (2004) and available at <http://lca.ucsd.edu/software/enzo/>.

following the cloud fragmentation and collapse until a density of  $10^5\text{cm}^{-3}$  and molecular hydrogen abundance of  $10^{-4}$  was reached. In Abel et al. (2002) the formation of molecular hydrogen via the three-body process was added, which extended the range of valid densities to  $n \lesssim 10^{10}\text{cm}^{-3}$  and allowed the collapse to continue until the formation of a fully molecular,  $\sim 1M_\odot$  protostar. No heating term for three-body  $\text{H}_2$  formation is included, an effect which can be important for the temperature evolution of the gas at  $n \gtrsim 10^9\text{cm}^{-3}$ . In this paper we focus on an intermediate regime at densities  $\sim 10^2 - 10^6\text{cm}^{-3}$  where the temperature is lowest. This regime is not sensitive to the high density core, and though we allow the simulations to continue to very high densities ( $\sim 10^{13}\text{cm}^{-3}$ ) we do not consider the core in our analysis.

In this work, we introduce three additional species to the network: D,  $\text{D}^+$ , and HD. Reaction rates for the deuterium species are listed in Table 1. A total of eight reactions are considered for the deuterium species. Five of the six reactions of the *minimal model* of Galli & Palla (1998) are included, using the updated rates from Galli & Palla (2002). We neglect photoionization of deuterium as we do not consider any external radiation fields other than the CMB, which does not contribute to this rate at  $z < 100$ . We include two additional deuterium reactions from Galli & Palla (2002) that were not part of the Galli & Palla (1998) minimal model. Lastly, we include deuterium ionization by collisions with electrons, for which the rate is unknown and the equivalent hydrogen rate is adopted (see, e.g., Glover & Jappens 2007).

The cosmological deuterium abundance is taken from Burles & Tytler (1998) and is  $\text{D}/\text{H} = 3.4 \times 10^{-5}$  (by number). This is  $\sim 40\%$  larger than the value obtained by Romano et al. (2003) using WMAP first-year results, though it is within the range of other D/H measurements (see Romano et al. 2003, Table 1).

We adopt the recently computed HD cooling function of Lipovka et al. (2005). Their rate calculation includes all radiative and collisional transitions for the  $J \leq 8$  rotational levels and the  $v = 0, 1, 2, 3$  vibrational levels. The rates are similar to previous formulations (e.g., Flower et al. 2000) except at high densities and temperatures ( $T \gtrsim 1000\text{K}$ ) where the collisional ro-vibrational transitions provide added cooling. From Lipovka et al. (2005), we use their equation 5 for the low-density limit, and in the LTE approximation we use the polynomial fit from their equation 4 with a density of  $n_{\text{H}} = 10^6\text{cm}^{-3}$  (at which point the cooling function has saturated). The high and low density limits are combined as

$$\Lambda(n_{\text{H}}, T) = \frac{\Lambda^{(\text{LTE})}}{1 + \frac{\Lambda^{(\text{LTE})}}{n_{\text{H}}\Lambda^{(n \rightarrow 0)}}}. \quad (1)$$

We prevent cooling below the CMB temperature by setting the HD cooling rate to zero when the temperature in a simulation cell falls below the CMB temperature at the current redshift.

Following Bromm et al. (2002) and Johnson & Bromm (2006), we verified the chemical network in Enzo by comparing the equilibrium abundances of the species most important for cooling against values derived analytically. While Enzo is designed primarily for cosmological sim-

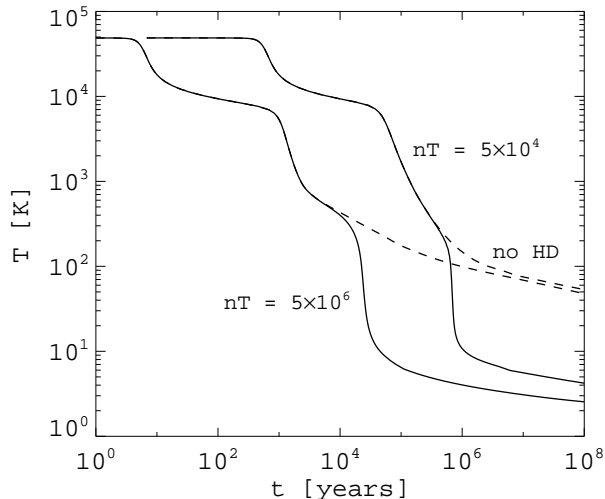


FIG. 2.— Thermal evolution of an ionized gas with an initial temperature of 50000K under isobaric conditions with and without HD cooling (solid and dashed lines, respectively). Once a temperature of  $\lesssim 300\text{K}$  is reached, HD cooling dominates and the gas cools to essentially to zero temperature, whereas gas with  $\text{H}_2$  cooling does not cool below  $\sim 60\text{K}$ . Note that this is not a cosmological simulation and heating from the CMB was not considered. The evolutionary phases of the gas are very similar to Figure 2 of Yoshida et al. (2007a), though the transitions occur on slightly different timescales due to the different rates used.

ulations, it is possible to set up idealized problems and study the physics in detail. We created an adiabatic steady-state model consisting only of baryonic gas at an initial temperature and density uniformly distributed within a static (non-expanding) volume, and with radiative cooling disabled. Using this setup, we ran simulations ranging in temperature from  $10^3\text{K} < T < 10^6\text{K}$  and allowed each simulation to run until the abundances of all 12 species converged. The results are shown in Figure 1; the simulation data are in excellent agreement with the values derived analytically in the appendix.

In addition to examining the equilibrium properties of an isothermal gas, we considered the temperature evolution of hot gas that is cooling isobarically. This simplified model approximates the conditions of photoionized gas as may be expected for relic HII regions, SNe bubbles, or the shock ionized regions of colliding halos. Using the setup described above, but with radiative cooling enabled and maintaining isobaric conditions by forcing  $nT$  to be a constant at each timestep, we followed the temperature evolution of the gas until a minimum temperature was reached. This test was motivated by the work of Yoshida et al. (2007a); comparison of our Figure 2 to their Figure 2 shows that similar results are obtained by two different numerical models. Figure 2 shows that HD cooling is important in ionized gas, lowering the minimum temperature to 10K (no radiative heating from the CMB was considered in this run).

### 2.2. Simulation Setup

The framework for our simulations is a single box 1 comoving Mpc on a side within a  $\Lambda\text{CDM}$  universe with cosmological parameters consistent with Spergel et al. (2007):  $\Omega_\Lambda = 0.76$ ,  $\Omega_m = 0.24$ ,  $\Omega_b = 0.041$ ,  $H_0 = 73 \text{ km/s/Mpc}$ , and  $\sigma_8 = 0.74$ . The box is partitioned into

a root grid of  $128^3$  elements and initialized at  $z = 99$  with  $128^3$  dark matter particles using an Eisenstein & Hu (1999) power spectrum with a spectral index of  $n = 0.95$ . The evolution of the dark matter particles is followed to  $z = 10$  using a low resolution run, then four of the most massive virialized halos are identified using the HOP algorithm (Eisenstein & Hut 1998).

Each of the four halos represents a potential site for primordial star formation. The particles identified with each halo at  $z = 10$  are traced to their positions at  $z = 99$ , and three additional levels of nested static subgrids are defined within the root grid such that all halo particles are contained within the highest resolution subgrid at all times (the highest resolution region has an effective resolution of  $1024^3$ ). The subgrids are centered on a given halo, so that while all the simulations share the same root grid and initial conditions, the high resolution subgrids are defined independently for each. The initial conditions are then regenerated to include both baryons and dark matter. In the highest resolution subgrid the dark matter particle mass is  $27.2 M_\odot$  and the average baryonic mass in each cell is  $5.6 M_\odot$ .

In the high resolution runs this innermost subgrid is further refined up to a maximum of 25 levels, with each refinement increasing the cell resolution by a factor of two along each axis. Cells are flagged for refinement whenever the baryonic or dark matter mass in a cell is more than 4 times the resolution masses quoted above (Truelove et al. 1997). In addition, a cell is refined if the cell width  $\Delta x$  is less than 0.25 times the local Jeans length. The dark matter density is smoothed on a scale of 1 comoving parsec in order to avoid heating of the baryons due to discreteness effects of the dark matter particles, as in Abel et al. (2002). When the simulations reach the maximum refinement level, the cell length within the highest refinement region is 46.1 AU and the gas mass resolution is  $9.7 \times 10^{-3} M_\odot$ .

For each halo, two runs are performed, one including HD chemistry and one without, to isolate the effects of HD cooling and facilitate comparison with previous simulations where HD was not included. We test the case of primordial star formation in ionized gas as discussed in the introduction by repeating the simulations for three of the halos while ionizing the full simulation volume at  $z = 20$ .

## 3. RESULTS

### 3.1. Unperturbed Primordial Gas

The first case we consider is for unperturbed primordial gas (Population III.1), beginning at  $z = 99$  and evolving normally until the formation of a protostar. For all eight runs ( $4 \times \text{H}_2 + 4 \times \text{HD}$ ) a core (proper) density of  $n \sim 10^3 \text{ cm}^{-3}$  is reached at  $z \sim 15$ , indicating the collapse of a protostellar seed. The  $\text{H}_2$  mass fraction quickly climbs to  $10^{-3}$  at a radius of  $\sim 1 \text{ pc}$  and effectively cools the gas, lowering the temperature to a minimum of  $\sim 300\text{K}$ . As the collapse continues, the density exceeds  $n \sim 10^4 \text{ cm}^{-3}$  and the  $\text{H}_2$  cooling rate becomes independent of density. The temperature of the contracting gas rises, and once a density of  $10^8 \text{ cm}^{-3}$  is reached  $\text{H}_2$  is formed rapidly through the three-body process until the core is fully molecular. The simulations are terminated when the core density exceeds  $n \sim 10^{13} \text{ cm}^{-3}$ , though

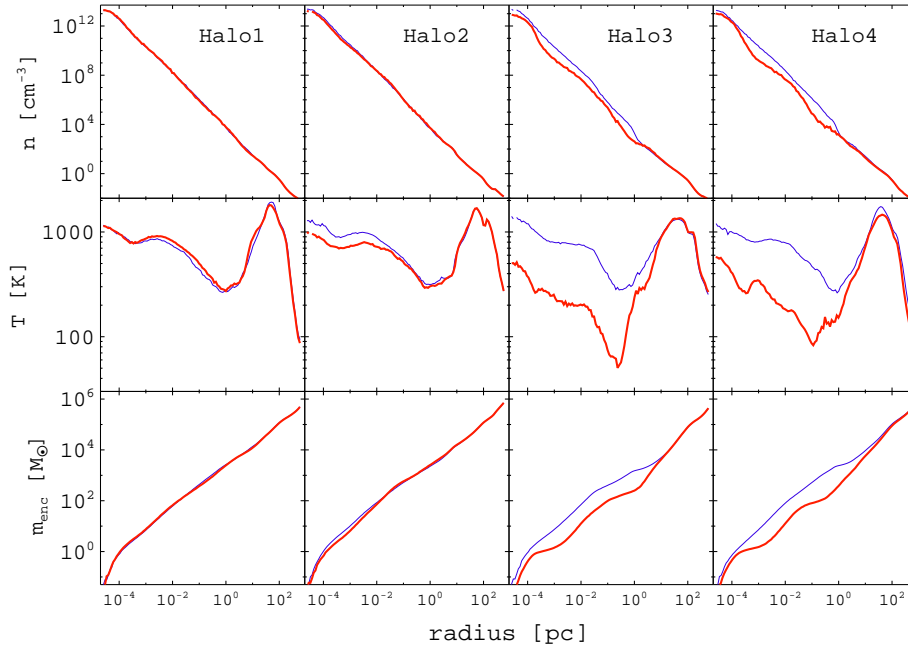


FIG. 3.— Radial profiles of gas properties at the final timestep for simulations with unperturbed primordial gas.  $\text{H}_2$  runs are indicated by thin blue lines and HD runs by thick red lines. The two more massive halos, Halo1 and Halo2, show little difference between runs with and without deuterium chemistry. The two less massive halos, Halo3 and Halo4, show significantly lower temperatures within the collapse region, and are also less dense within the inner parsec.

we do not consider the inner core in detail and restrict our discussion to densities  $< 10^{10} \text{ cm}^{-3}$  (see §2.1). The inner  $\sim 20$  AU contains a fully molecular  $\sim 1M_{\odot}$  protostar, consistent with the results of Abel et al. (2002).

Properties of the individual halos are given in Table 2. The four halos span a factor of  $\sim 2$  in virial mass. At the virial scale, HD has little effect on the halo gas. The collapse to a protostar occurs at similar redshifts and virial temperatures whether HD is included or not. However, the properties of the halo gas well inside the virial radius, particularly in the region where the minimum temperature is reached, are clearly affected for two of the four halos, as is evident in the radial temperature profiles of all four halos (Figure 3). Within  $\sim 3$  parsecs, the  $\text{H}_2$  and HD runs for Halo3 and Halo4 diverge, with the HD runs having lower average densities and temperatures compared to the  $\text{H}_2$  runs. This indicates that HD cooling is effective in these halos, while for the other two halos it is not.

Figure 4 shows that throughout most of the collapse region, HD production closely follows  $\text{H}_2$  production with a factor of  $10^{-4}$  reduction in number density. The exception is a region of enhanced HD production in a spherical shell  $\sim 1$ pc from the core, corresponding to the minimum temperature. For Halo1 and Halo2, the HD/ $\text{H}_2$  ratio reaches a maximum of  $\sim 2 \times 10^{-4}$  in this region, and HD cooling contributes less than 20% of the overall cooling, which is governed by  $\text{H}_2$  (Figure 5). On the other hand, for Halo3 and Halo4 the maximum HD/ $\text{H}_2$  ratio is  $\sim 10^{-3}$  and HD provides more than 90% of the total cooling at densities of  $10^5 \text{ cm}^{-3} \lesssim n \lesssim 10^7 \text{ cm}^{-3}$ . HD cools more effectively than  $\text{H}_2$  at low temperatures; when HD cooling is dominant the minimum gas temperature drops from  $\sim 300\text{K}$  to  $\lesssim 100\text{K}$ .

Interestingly, in the two HD-cooling halos the overall cooling is reduced, as can be seen in the ratio of the cool-

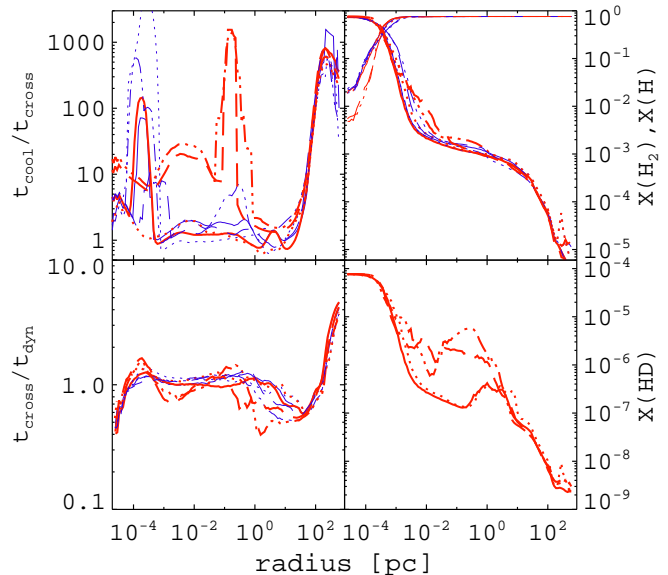


FIG. 4.— Upper left: ratio of cooling time to crossing time for all 8 runs, with  $\text{H}_2$  runs in thin blue lines and HD runs in thick red lines. Halo1 is shown as solid lines, Halo2 as dotted lines, Halo3 as dashed-dotted lines, and Halo4 as long dashed lines. The cooling time is much greater in the Halo3-HD and Halo4-HD runs where HD cooling is efficient due to the reduced cooling efficiency at low temperatures. Lower left: ratio of crossing time to dynamical time, which is very close to one for all cases and indicates dynamical stability. Upper right: mass fractions of  $\text{H}_2$  and H. The fraction of molecular hydrogen approaches unity within the innermost part of the cloud. Lower right: mass fraction of HD, which is enhanced by a factor of 20-50 in the Halo3-HD and Halo4-HD runs.

ing time to crossing time (Figure 4). Near the temperature minimum, the cooling time rises dramatically for the HD-cooling halos, as the gas temperature is near the CMB temperature and the cooling rate goes to zero. In-

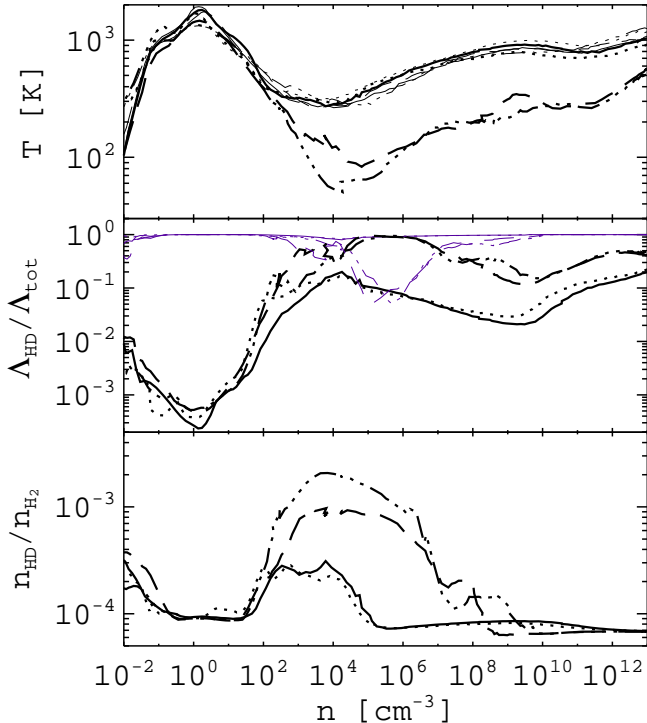


FIG. 5.— Contribution of HD to the total cooling in the HD runs. Line styles used for each halo are described Figure 4. The top panel shows temperature as a function of density. For reference, the results from H<sub>2</sub> runs are shown with thin lines. The middle panel shows the contribution to the total cooling from HD, with thin lines showing the contribution of H<sub>2</sub> cooling in the HD runs. The bottom panel shows the HD/H<sub>2</sub> ratio, indicating where fractionation has occurred. For Halo1 and Halo2, HD provides  $\lesssim 10\%$  of the total cooling the gas, while for Halo3 and Halo4, the HD/H<sub>2</sub> ratio is greater by 3–5 $\times$  and HD provides  $\gtrsim 90\%$  of the total cooling over a wide range in density.

side this region, the temperature rises while the HD/H<sub>2</sub> ratio drops. Thus in the inner part of the cloud the gas remains cool ( $T \gtrsim 250\text{K}$ ) but there is less HD, so that the overall cooling remains low ( $t_{\text{cool}}/t_{\text{cross}} \sim 20$ )<sup>3</sup>. The decrease in gas temperature caused by HD cooling actually reduces the total cooling rate, so that the gas will contract quasi-statically.

An obvious difference is that the two halos with effective HD cooling have the two lowest masses (somewhat below  $10^6 M_{\odot}$ ), while the two H<sub>2</sub> cooling halos have masses around  $10^6 M_{\odot}$  or more. Ripamonti (2007) noted that halos below  $\sim 3 \times 10^5 M_{\odot}$  collapse more slowly because H<sub>2</sub> is not produced in sufficient quantities to efficiently dissipate the heat generated by gravitational contraction. The slower collapse allows HD to build up until it becomes a substantial coolant. This is similar to the results of Bromm et al. (2002), who simulated a  $2 \times 10^5 M_{\odot}$  halo with HD cooling that went through an extended phase of quasi-hydrostatic contraction and cooled to lower temperatures. In both of these studies, when more massive ( $> 10^6 M_{\odot}$ ) halos were tested with and without HD chemistry, HD was found to have little effect. We find that halos as massive as  $8 \times 10^5 M_{\odot}$  generate substantial HD cooling, but do not take longer

<sup>3</sup> The cooling time is defined as  $E/\dot{E}$  and the crossing time as  $r/c_s$ . Both are locally defined within a grid cell.

to collapse. In both Ripamonti (2007) and Bromm et al. (2002), idealized conditions of a single halo were considered, whereas in our simulations the full merger history of a halo is treated self-consistently. Thus we must examine the evolution of the gas in more detail to understand why HD cooling is effective in low mass halos.

We find that HD cooling in unperturbed primordial gas is a highly sensitive process. Two effects combine to

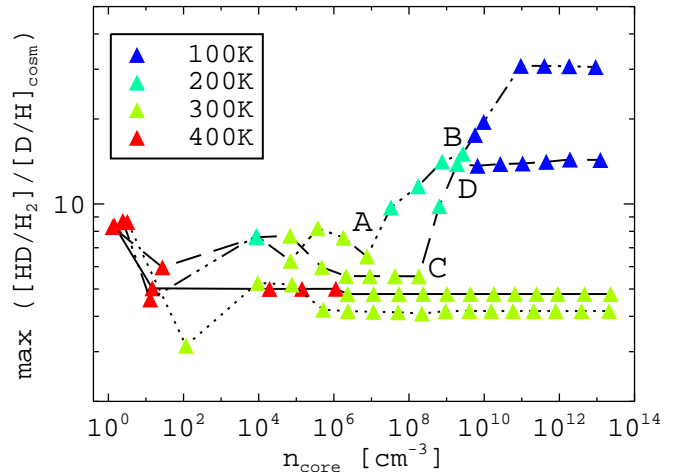


FIG. 6.— Evolution of the HD/H<sub>2</sub> abundance ratio relative to the cosmological D/H abundance ratio during the collapse (the maximum enhancement within the collapse region is plotted). The x-axis represents the core density, and each halo is followed once a core density of  $1 \text{ cm}^{-3}$  is reached. Linestyles are as in Figure 4. Filled symbols correspond to individual output times, with the color representing the minimum temperature in the collapse region at that time. In equilibrium, the HD enhancement would be  $\sim 6$  at 250K and  $\sim 100$  at 100K. The strong HD enhancement in two of the halos only occurs after the core density has exceeded  $\sim 10^8 \text{ cm}^{-3}$  and the temperature has remained  $\lesssim 200\text{K}$ . For Halo3, the HD enhancement increases from 6.5 at point A to 15 at point B, a time span of 0.7 Myr. Halo4 undergoes an increase in HD enhancement from 5.5 (point C) to 14 (point D) within 0.3 Myr. While Halo3 continues to increase in HD enhancement, for both halos this brief period of strong enhancement signals the point at which HD cooling goes from marginal to significant importance.

drive the effectiveness of HD cooling in low temperature primordial gas. First, the primary formation channel for HD,



is endothermic by 462K, so that HD formation is favored over H<sub>2</sub> by a factor  $e^{462/T}$  (Glover 2007). Second, the HD cooling rate per molecule is greater than that of H<sub>2</sub> below a critical temperature. This critical temperature is determined by the gas density and the abundances of H<sub>2</sub> and HD, and is generally in the range 150-250K (see the discussion and Figure 1 in Glover 2007). Should H<sub>2</sub> cool the gas to the critical temperature, HD cooling will become important and can cool the gas even further. This results in a runaway effect, as HD is formed rapidly in the cool gas.

Indeed, we do not see a slow buildup of HD as in Ripamonti (2007); rather, the HD enhancement occurs rapidly in the latter stages of the collapse. Figure 6 shows the HD enhancement in each of the four halos, expressed in terms of the HD/H<sub>2</sub> abundance ratio divided by the cosmological D/H abundance ratio (both



values are ratios of number densities, the cosmological D/H value is stated in §2.1). At an early stage in the

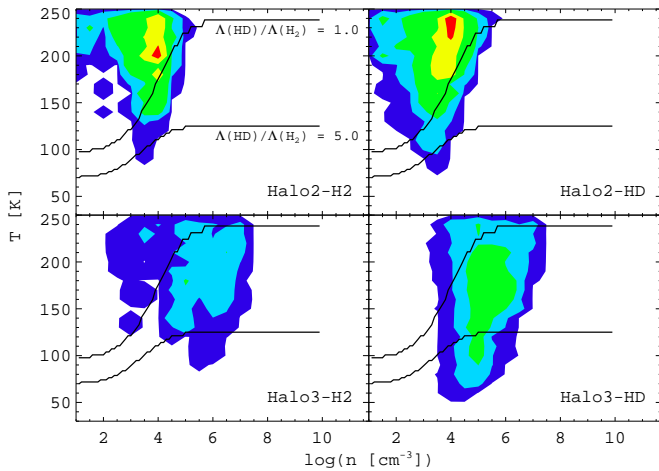


FIG. 7.— Distribution of the gas in the  $n - T$  plane for two halos, at a time when the central density is  $\sim 5 \times 10^7 \text{ cm}^{-3}$ . Contours represent fractions of  $(0.1, 2.5, 10, 100) \times 10^{-6}$  of the halo virial gas mass, which is  $\sim 10^6 M_\odot$  for Halo2 and  $\sim 7 \times 10^5 M_\odot$  for Halo3. The upper line shows the critical temperature at which the HD cooling rate per unit volume is equal to the  $\text{H}_2$  cooling rate, calculated at the corresponding density and temperature and assuming that  $n_{\text{H}_2} = 10^{-3} n_{\text{H}}$  and  $n_{\text{HD}} = 3 \times 10^{-4} n_{\text{H}_2}$ , which are typical values for the gas in these regions (see Figure 5). The lower line shows the temperature at which HD provides 5 times the cooling of  $\text{H}_2$ . The upper panels show the gas distribution for both the  $\text{H}_2$  (left panel) and HD (right panel) runs of Halo2. Most of the gas is above the critical region; this halo does not exhibit effective HD cooling. The lower panels show that for Halo3 the cool gas is shifted to higher densities and a much greater amount of gas is within the critical region; this halo does exhibit effective HD cooling.

collapse, when the core density is  $\sim 1 \text{ cm}^{-3}$ , the maximum HD enhancement is  $\sim 8$  for all halos. When Halo3 reaches point A, the minimum temperature is 220K, and the HD enhancement is still only 6.5. Within 0.7 Myr, point B is reached, where the minimum temperature has dropped to 150K, and the HD enhancement has jumped to 15. Halo4 undergoes a similar process, at point C the minimum temperature is 225K and the HD enhancement is 5.5, but 0.3 Myr later at point D the temperature has dropped to 100K and the HD enhancement is 14. Both halos collapse from  $n_{\text{core}} = 1 \text{ cm}^{-3}$  to  $n_{\text{core}} = 10^{13} \text{ cm}^{-3}$  in  $\sim 100$  Myr, thus most of the HD enhancement occurs in less than 1% of the total collapse time. In fact, we find that HD cooling exhibits a ‘critical’ nature, in the sense that either HD cooling is very important to the cooling or it is not important at all. This behavior stems from the rapid HD fractionation and the runaway effect of cooling.

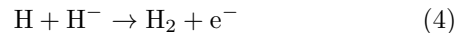
The conditions for effective HD cooling are then that the gas must cool by  $\text{H}_2$  cooling to the critical temperature and remain there long enough for a buildup of HD to occur. This is most likely to occur in lower mass halos. Halos with large gravitational potentials have higher virial temperatures and more dynamical activity. Mergers from infalling gas clumps will disrupt pockets of cool gas. Lower mass halos, which collapse more uniformly, are better able to form dense pockets of cool gas where HD can form.

We also find evidence for the critical nature of HD

cooling by looking in detail at the low temperature gas in our simulations. Figure 7 shows the  $n - T$  plane for Halo2 and Halo3 at a time when the central density is  $5 \times 10^7 \text{ cm}^{-3}$ , just before the large HD enhancement seen in two of the halos (Figure 6). It is clear that the lower mass halo, Halo3, has much more gas at higher densities ( $\sim 10^5 \text{ cm}^{-3}$ ) and low temperatures ( $T < 200 \text{ K}$ ) than Halo2. This gas is well below the critical temperature and is cooling effectively by HD. While some gas in the more massive Halo2 is just below the critical line, most of it remains above and HD cooling is not effective for this halo. Our results, combined with the findings of Ripamonti (2007) and Bromm et al. (2002), suggest that a set of conditions must be met for effective HD cooling in unperturbed primordial gas, and these conditions are most likely to occur in  $< 10^6 M_\odot$  halos.

### 3.2. Primordial Star Formation in Ionized Regions

The second case we consider is primordial star formation in ionized regions (Population III.2). In sites of primordial star formation, molecular hydrogen forms primarily through the  $\text{H}^-$  channel,



a reaction which is catalyzed by free electrons and thus enhanced in ionized gas. Ionized primordial gas could be found in shocks from colliding massive halos, or in the photoionized regions surrounding the first generation of stars. The latter case is of particular interest, as the end state of  $\gtrsim 100 M_\odot$  primordial stars is probably either direct collapse to black holes or complete destruction in pair instability supernovae (Heger et al. 2003). In either case a sizable HII region will result, and as the first stars themselves form in large overdensities these fossil HII regions will host dense gas clouds that could be sites for subsequent star formation. As  $\text{H}_2$  forms rapidly in the ionized regions, the gas cools to  $T \sim 100 \text{ K}$ , where HD formation is highly favored and HD cooling can drive the temperature even lower, essentially to the CMB temperature. The resulting low Jeans masses imply lower mass stars (Nagakura & Omukai 2005; Johnson & Bromm 2006).

We explore the formation of primordial stars in ionized gas through the simple approach of ionizing the entire simulation volume at  $z = 20$ . This technique has been similarly utilized with Enzo by O’Shea et al. (2005) but without HD chemistry. While this method is not equivalent to a full treatment of radiative transfer, it does allow us to examine in detail the effect of HD cooling in ionized regions for otherwise identical halos, while being much less expensive computationally.

We used three of the simulation volumes described in § 2.2, so that the evolution to  $z = 20$  is identical to the unperturbed case (§ 3.1), but the late stage evolution begins with a high abundance of free electrons. As previously, the simulations are performed once without HD chemistry and once with HD included.

Table 3 shows the properties of the halos for the ionized runs. Compared to the unperturbed case (Table 2), the collapse for a given halo occurs somewhat earlier and at lower virial masses and temperatures in ionized regions. The resulting density, temperature and enclosed mass

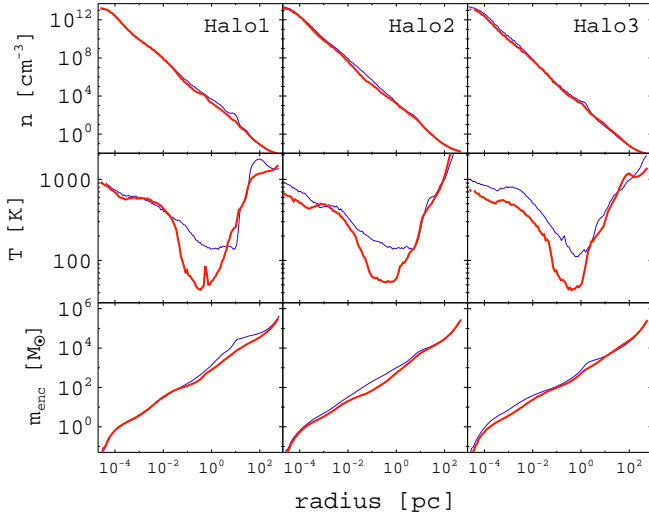


FIG. 8.— The same as Figure 3 but for the flash-ionized runs. Similar results are found for the three halos examined, in all cases temperature minimum approaches the CMB temperature at the redshift of collapse.

profiles are shown in Figure 8. As in Figure 3, the HD simulations show distinctly lower temperatures than the H<sub>2</sub> runs in the range 0.01 - 10 pc, but now the effect is independent of mass.

In Figure 9 it is clear that the molecular hydrogen fraction is greatly enhanced over the unperturbed case as expected. The extra H<sub>2</sub> lowers the gas temperature to  $\sim 130$ K even without HD cooling, a factor of  $\gtrsim 2$  lower than achieved in the H<sub>2</sub> cooling unperturbed halos. When HD chemistry is included, it forms rapidly in the low temperature gas. This can be seen in the

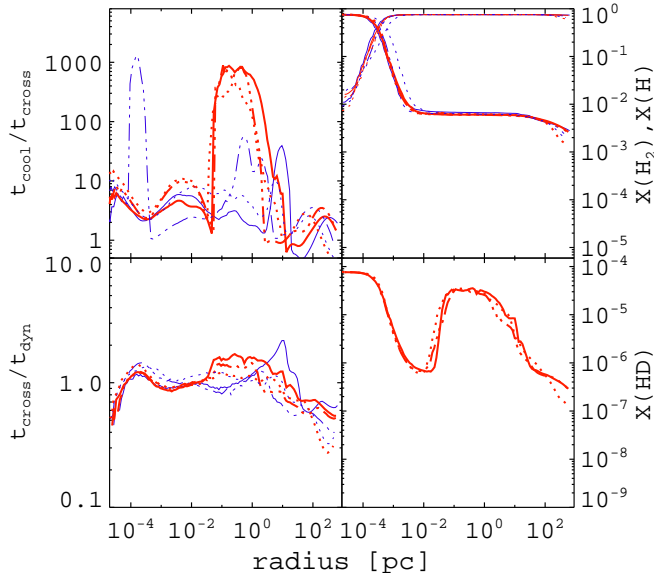


FIG. 9.— The same as Figure 4 but for the flash-ionized runs. The molecular hydrogen abundance is  $> 10^{-3}$  throughout due to the enhancement of the H<sup>-</sup> channel by the free electrons. The cloud is dynamically stable ( $t_{\text{cross}}/t_{\text{dyn}} \sim 1$ ). HD is greatly enhanced within 1pc, where  $T \sim 100$ K.

large bump in the HD fraction at  $\sim 1$ pc, which reaches a maximum of  $4 \times 10^{-5}$ , nearly two orders of magnitude

greater than seen in the unperturbed halos. As a result, the temperature is driven to the CMB floor, and HD provides  $> 95\%$  of the total cooling in the low temperature zone (Figure 10).

It is interesting to compare the radial development of the H<sub>2</sub> and HD abundances shown in Figure 9. Moving inward from a radius  $\sim 100$ pc, the H<sub>2</sub> mass fraction rises to a maximum of  $\sim 6 \times 10^{-3}$ , and remains essentially constant until a radius of  $\sim 10^{-3}$ pc. On the other hand, the HD mass fraction steadily rises from  $\sim 100$ pc to  $\sim 1$ pc, as the temperature drops from  $\sim 1000$ K to  $\sim 100$ K. Over the next decade in radius, the tempera-

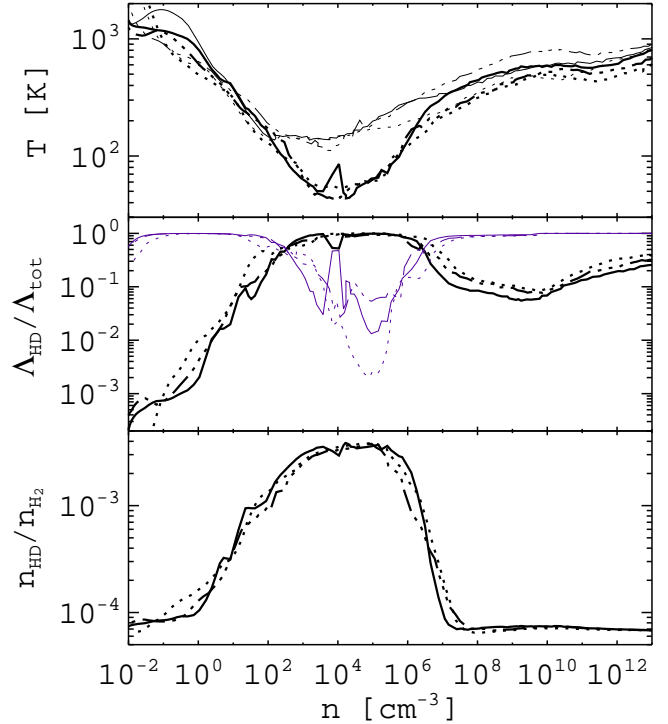


FIG. 10.— The same as Figure 5 but for the flash-ionized runs. Note that HD cooling is now important for all halos, accounting for 95-99.7% of the cooling in the  $T < 100$ K region.

ture is roughly constant near the minimum, and the HD mass fraction remains at its peak of  $\sim 3 \times 10^{-5}$ . In this region HD fractionation is nearly complete, and the HD/H<sub>2</sub> ratio reaches  $4 \times 10^{-3}$  (Figure 10). At a density of  $\sim 10^6 \text{cm}^{-3}$ , the HD cooling function saturates and the temperature rises, leading to a sharp drop in the HD abundance, while the H<sub>2</sub> abundance is still roughly constant. In the inner 0.01pc, H<sub>2</sub> forms rapidly through the three-body process while the temperature again climbs to  $\gtrsim 700$ K, so that the HD abundance again follows the H<sub>2</sub> abundance reduced by a factor of  $7 \times 10^{-5}$ .

## 4. DISCUSSION

### 4.1. General effects of HD cooling

In general, HD cooling is only important once H<sub>2</sub> cooling has lowered the gas temperature to  $\sim 200$ K. This only occurs once the gas is already quite dense ( $n \sim 10^4 \text{cm}^{-3}$ ). Thus HD cooling does not affect which halos will form stars, but it does alter the properties of the gas in the



region of the temperature minimum.

For halos with effective HD cooling, the minimum temperature is not only lowered by a factor of a few compared to runs without HD, the location of the minimum is shifted to a smaller radius and hence higher densities. When  $\text{H}_2$  cooling dominates the minimum temperature occurs at a density of  $n \sim 10^3 - 10^4 \text{cm}^{-3}$ . When HD cooling dominates, the minimum temperature occurs at a density of  $n \sim 10^4 - 10^5 \text{cm}^{-3}$ .

This effect is easily understood by considering the properties of the  $\text{H}_2$  and HD cooling functions. First, it is useful to assume that the gas is thermally balanced with heating due to gravitational collapse balancing radiative cooling. The gravitational energy input rate per unit volume can be approximated as

$$n \left( \frac{GM(r)}{r} \right) t_{\text{dyn}}^{-1} \propto n^{3/2}. \quad (5)$$

To derive this simplified expression, we have assumed that the enclosed mass  $M(r)$  is proportional to  $r$ , or alternately that  $\rho(r) \propto r^{-2}$ , as can be seen in Figures 3 and 8. The dynamical time  $t_{\text{dyn}} \propto n^{-1/2}$ .

Over a short range in temperature, the cooling function can be roughly approximated as

$$\Lambda \propto \begin{cases} n^2 T^\alpha & (n < n_{\text{cr}}) \\ n T^\alpha & (n > n_{\text{cr}}) \end{cases} \quad (6)$$

depending on whether the density  $n$  is above or below the critical density  $n_{\text{cr}}$ . For both the  $\text{H}_2$  and HD cooling curves,  $\alpha$  is quite large, typically of order 3-5 in the interesting range. By equating these two expressions for the heating and cooling we can derive a relation between density and temperature. When we do this, we see that the temperature reaches a minimum at the critical density, where it transitions from  $T \sim n^{-0.5/\alpha}$  to  $T \sim n^{0.5/\alpha}$ . The critical density for  $\text{H}_2$  is  $n \sim 10^3 - 10^4 \text{cm}^{-3}$ , while for HD it is  $n \sim 10^5 - 10^6 \text{cm}^{-3}$  (Lipovka et al. 2005; Flower et al. 2000). This explains the shift in the location of minimum temperature to higher densities as seen in Figures 5 and 10 (and Tables 2 and 3). In addition, the high value of  $\alpha \sim 4$  explains the relatively flat temperature profiles seen in the simulations. The increase in the temperature at densities beyond the critical density ultimately leads to a shutoff of HD cooling and, as we see in the next section, important implications for the masses of the resulting stars.

#### 4.2. Masses of the First Stars

We have shown that HD cooling can be as important as  $\text{H}_2$  cooling for some low mass primordial gas clouds and in ionized regions. We can now examine whether HD cooling changes the nature of the collapse enough to alter the mass function of the first stars. Figure 11 shows the accretion timescales for all simulations, calculated according to the Shu isothermal model (Shu 1977), where  $\dot{m} = 0.975c_s^3/G$  (we obtain similar but noisier results using the instantaneous mass inflow rate,  $\dot{m} = 4\pi r^2 v_r \rho$ ).

For primordial halos, the accretion times are similar for all of the  $\text{H}_2$  cooling halos, suggesting  $\sim 300M_\odot$  stars will form after  $10^5$  years of accretion. However, the two HD cooling halos accrete significantly less mass for a given accretion time. This results from the de-

creases in temperature and enclosed mass at  $r \sim 1\text{pc}$  when HD cooling is effective. This is an important scale for star formation as this is the region at which the Bonner-Ebert mass is at a minimum. Our results suggest that stars of  $\sim 50M_\odot$  will form, much lower than is typically seen in simulations of first generation star formation. We conclude, in agreement with Ripamonti (2007), that there are two mass scales for the first stars. Some (most) stars will form in halos of  $10^6 M_\odot$ , cool by  $\text{H}_2$ , and have masses  $> 100M_\odot$ . The remainder will form in less massive halos, cool by HD, and have masses  $< 100M_\odot$ . According to Heger et al. (2003), metal-free

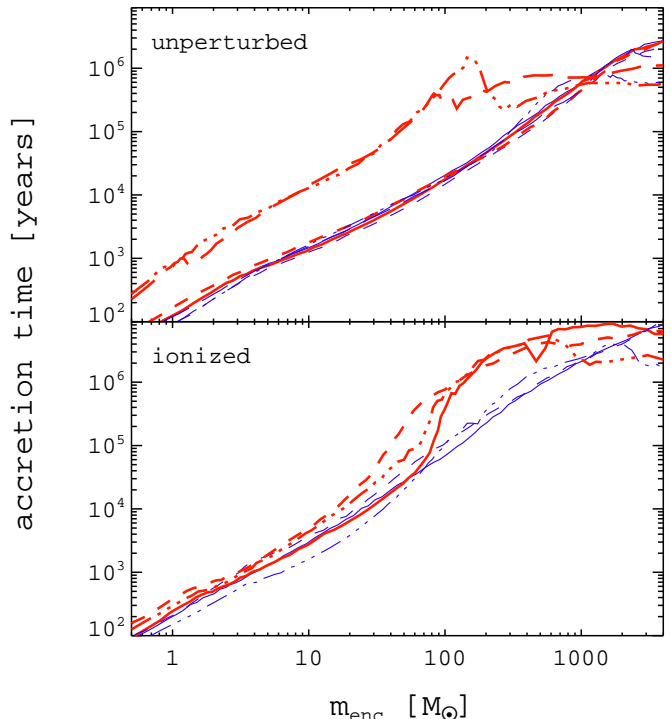


FIG. 11.— Accretion times onto protostars in all simulations calculated using the Shu rate, with  $t_{\text{acc}} = m/\dot{m}$ . Linestyles are the same as Figure 4. The upper panel shows results from the unperturbed runs, while the lower panel shows results from the ionized runs. In the unperturbed case, HD has little effect on the expected final mass for the stars in Halo1 and Halo2, while having a strong effect for Halo3 and Halo4. The accreted mass is reduced by a factor of  $\sim 6$ . In the ionized case, HD cooling reduces the accreted mass by  $\lesssim 2$ . The mass scale for primordial halos with effective HD cooling is quite similar to that of ionized halos.

stars with masses  $> 100M_\odot$  will produce pair-instability supernovae, while those with masses  $40-100M_\odot$  will collapse directly to black holes. Thus HD cooling may be important in setting the mass scale of the first stars and in the later evolution of the interstellar medium.

The inner regions of the ionized halos are quite similar in density and temperature, but when HD cooling is included the temperature is lower by a factor of  $\gtrsim 2$ . The accreted mass is affected by a similar amount; the lower panel of Figure 11 shows that HD cooling lowers the expected mass of primordial stars in ionized regions from  $\gtrsim 100M_\odot$  to  $\sim 60M_\odot$ . This mass scale agrees well with the results of Yoshida et al. (2007b), who examined the development of a protostar in a primordial III

region with SPH simulations that included HD chemistry. They followed the evolution of the protostar to a central density of  $10^{18}\text{cm}^{-3}$  including a detailed protostellar evolution model that traced the evolution to the zero-age main sequence. They predicted that a  $\sim 40M_{\odot}$  star would form in the HII region, more massive than earlier simulations had predicted. Our finding of a similar mass scale for three different halos suggests that while second generation primordial stars are not as massive as the first generation, they are still quite massive.

We note that extrapolating a final stellar mass from estimations of the accretion rate is highly uncertain and some caution should be taken in interpreting the stellar masses. It is unclear whether a direct relationship exists between accretion rate and final stellar mass, whether the accretion is spherical (Omukai & Palla 2003) or through an accretion disk (Tan & McKee 2004; McKee & Tan 2007). Taking these uncertainties into consideration, it is clear that HD cooling has a significant effect on both the temperature and density evolution of lower mass Population III.1 halos. The total mass within a given radius is much lower when HD cooling is effective (Figure 3), implying stars of much lower mass will form. In ionized halos, the differences are much smaller (Figure 8), implying that in this case the resulting stars will not be significantly less massive.

We do not see signs of fragmentation in projections of the inner collapse regions. We also do not see evidence for the formation of rotationally-supported disks, as  $v_{\text{circ}}/v_{\text{kep}} < 1$  in all our simulations. This is not a surprise, as we do not expect HD cooling to cause fragmentation – like  $\text{H}_2$  it has a steep cooling function and so is stable to thermal instabilities. In addition, as we see in Figure 9, the cooling time never drops below the dynamical time, another important criterion for fragmentation.

#### 4.3. Rate uncertainties

The results presented here depend on the accuracy of the chemical model. We showed in § 2.1 that the chemistry solver numerically reproduces the expected abundances in equilibrium; however, the calculated values are only as accurate as the rates given as input. Glover et al. (2006) and Glover (2007) have noted that two of the rates most strongly tied to  $\text{H}_2$  formation are also the most uncertain (see also Glover & Abel 2008). The first, the  $\text{H}^-$  channel, is less relevant to the unperturbed case but may be important in ionized regions. This uncertainty will propagate into simulations with HD, as HD primarily forms through  $\text{H}_2$ . As discussed in Glover et al. (2006), this can be an important source of uncertainty in these calculations, and we reiterate the need for improved rate measurements and calculations.

The second uncertainty discussed by Glover (2007) is in the three-body  $\text{H}_2$  formation process. This uncertainty will not qualitatively affect our results, as the three-body process is only important in the inner core of the collapse region, where the temperature climbs up to  $\gtrsim 500\text{K}$  and HD is less important. We did not include an analogous three-body process for HD formation, though for the same reason we do not expect this to be an important process.

Another source of uncertainty is in the cosmological D/H ratio. As discussed in § 2.1, there is a factor  $\sim 2$  uncertainty in cosmological measurements of this value.

Figure 6 shows that HD cooling halos undergo a rapid fractionation phase; this is unlikely to be sensitive to small changes in the cosmological deuterium abundance. In addition, the final amount of HD enhancement differs by a factor of 2 for the HD cooling halos, yet the fraction of cooling from HD is similar for both cases (Figure 6).

## 5. CONCLUSIONS

In this paper, we have implemented a minimal chemical network for tracking the formation of HD in the Enzo cosmological hydrodynamics code. We have verified the network using both equilibrium and non-equilibrium tests and then applied this to the formation of primordial stars in high-redshift halos with cosmological initial conditions. We examined a range of halos under two different assumptions for the initial electron fraction. In the first case, the halos were unperturbed, with an initial electron fraction as predicted by standard cosmological evolution in the absence of ionizing backgrounds. As in previous work, the first collapsed objects form in  $10^{5-6} M_{\odot}$  halos at  $z \sim 15$ . In the second case, we ionized the halos at  $z = 20$  to investigate the impact of free electrons on the collapse. Although this simple ‘flash’ ionization is not a realistic description of, say, a nearby photoionization source, it does allow us to investigate the impact of HD cooling in the presence of a source of free electrons. Our primary results are as follows.

- For Population III.1 star formation in high mass halos (roughly  $10^6 M_{\odot}$  and above), HD cooling is unimportant. However, for the lower mass halos in our sample there was a factor of 10-100 increase in the HD fraction (compared to the high mass halos). This, in turn, caused HD cooling to dominate  $\text{H}_2$  cooling over the density range  $10^4 \text{cm}^{-3}$  to  $10^7 \text{cm}^{-3}$  (corresponding approximately to  $10^{-2}$  pc to 1 pc, in radii). The HD cooling permitted gas to reach nearly down to the CMB temperature.
- We found that in order for HD cooling to be important, a sufficient amount of gas needed to be at a low enough temperature and a sufficiently high density for HD to form preferentially over  $\text{H}_2$ . However, once this critical line was crossed, rapid HD fractionation coupled with runaway cooling quickly led HD to dominate the cooling rate. This requirement for lower temperatures helps to explain why low mass halos formed HD preferentially over high mass halos.
- For the ionized case (Population III.2), HD cooling was important in all halos examined regardless of mass. HD cooling was efficient enough for gas to reach the CMB temperature over an even larger range of radii.
- In all cases, once the density increased above the HD critical density (around  $10^{5-6} \text{cm}^{-3}$ ), the temperature began to rise again and invariably increased by about  $\sim 500 \text{K}$ , leading to the suppression of HD relative to  $\text{H}_2$ . This means that the interior solution ( $r < 10^{-2}$  pc) relies only on  $\text{H}_2$  cooling and so looks quite similar to the no-HD case. In addition, no sign of fragmentation was found.

- Despite the fact that HD cooling led to lower temperatures (often down to the CMB temperature), we found that the impact on the predicted mass accretion rates was relatively mild. It was largest for the unperturbed case, where the low mass halos were predicted to form stars a factor of six times lower than the no-HD case (from  $\sim 300M_{\odot}$  to  $\sim 50M_{\odot}$ , assuming an accretion time of  $10^5$  years – see §4 for a discussion of the uncertainties in accretion mass estimates). For the ionized case, the predicted accretion rates were nearly identical with and without HD, leading to at most a factor of two reduction in the mass of the predicted stars forming out of ionized regions (from  $\sim 100M_{\odot}$  to  $\sim 50M_{\odot}$ ).

These results have a number of interesting implications. First, they suggest a way for at least some relatively lower mass stars to form in primordial (or near primordial) halos, as some interpretations of the observed extremely low metallicity halo stars have required (Tumlinson 2007; Komiya et al. 2007). However, they also indicate that HD cooling by itself will not form substantially lower mass stars (e.g. by a factor of ten) as some previous analytic work has suggested. In particular, we have not found any sign of a new class of Population III.2 objects (at least for the initial conditions surveyed).

Our work suggest two avenues of future research. The first is a more careful and systematic investigation of the conditions for HD cooling in “unperturbed” halos. While our results indicate that HD cooling is more important in low mass halos, it is not clear how this depends on merger histories or stochastic effects. More work is required to find the fraction of halos which form via the HD channel for a complete sample of halos. In the ionized case, our methodology for introducing free electrons was deliberately simple. It would be useful to examine more realistic ionization modalities (e.g., Wise & Abel 2007; Yoshida et al. 2007a).

GB acknowledges support from NSF grants AST-05-07161, AST-05-47823, and AST-06-06959, as well as computational resources from the National Center for Supercomputing Applications. We would like to thank the referee for many helpful suggestions which greatly improved the clarity of the paper. We also thank Tom Abel, Simon Glover, Zoltan Haiman, Mordecai Mac-Low, and Dan Whalen for useful discussions.

## APPENDIX

In this appendix we show the derivation of the analytical formulas used to test the equilibrium abundances of the chemical network, as described in § 2.1 and shown in Figure 1. The chemical network for all reactions not involving deuterium is taken from the work of Abel et al. (1997). The complete set of reactions and their associated rates are given in that work, for brevity we focus here on the species most relevant to cooling in the primordial gas. For ease of comparison, rates listed in this appendix are also denoted R#, with the number corresponding to the rate number used in Abel et al. (1997) (and also within the Enzo source code).

The equilibrium abundance of ionized hydrogen is calculated from the collisional balance of  $H^+$  (Abel et al. (1997) rates R1-R2):



By assuming  $n_e = n_{H^+}$ , we derive

$$n_{H^+} = \frac{k_1}{k_2} n_H. \quad (3)$$

The abundance of neutral hydrogen is found by assuming  $n_{H,tot} = n_H + n_{H^+}$ .

The two processes for creating molecular hydrogen include the dominant  $H^-$  channel and charge exchange with  $H_2^+$  (rates R8 and R10),



The three processes governing the destruction of  $H_2$  are the reverse of the above charge exchange reaction, as well as collisional dissociations by electrons and neutral hydrogen (R11-R13),



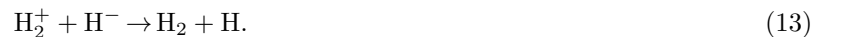
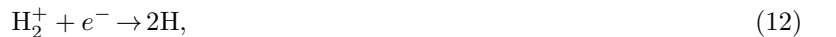
Thus the equilibrium abundance of  $H_2$  is given by

$$n_{H_2} = \frac{k_8 n_H n_{H^-} + k_{10} n_H n_{H_2^+}}{k_{11} n_{H^+} + k_{12} n_e + k_{13} n_H}. \quad (9)$$

Although the  $H_2$  abundance in the low-temperature gas ( $T < 10^4 K$ ) typical of primordial star formation is dominated by the  $H^-$  channel, we do not neglect  $H_2^+$  in our equilibrium calculation as it is important at higher temperatures. In addition to reaction (6) (also denoted R11), the following two reactions produce  $H_2^+$  (R9 and R17):



$H_2^+$  is destroyed by reaction (5) (also denoted R10) and the following reactions (R18, R19):



The equilibrium abundances for  $H_2$  and  $H_2^+$  are found by solving equation (9) simultaneously with

$$n_{H_2^+} = \frac{k_9 n_H n_{H^+} + k_{11} n_{H^+} n_{H_2} + k_{17} n_{H^-} n_{H^+}}{k_{10} n_H + k_{18} n_e + k_{19} n_{H^-}}. \quad (14)$$

$H^-$  is an important intermediary in the formation of  $H_2$ . It is formed primarily by photo-attachment of  $H$  and  $e^-$  (R7),



$H^-$  is destroyed in a series of collisional processes, including reaction (11) (also denoted R17) and the following rates (R14-R16):



This leads to the equilibrium equation

$$n_{\text{H}^-} = \frac{k_7 n_{\text{H}} n_e}{k_8 n_{\text{H}} + k_{14} n_e + k_{15} n_{\text{H}} + k_{16} n_{\text{H}^+} + k_{17} n_{\text{H}^+}}. \quad (19)$$

From Table 1,  $\text{D}^+$  is primarily created by collisional ionization and destroyed by recombination and collision with neutral hydrogen,

$$n_{\text{D}^+} = \frac{k_{50} n_{\text{D}} n_{\text{H}^+}}{k_2 n_{\text{H}^+} + k_{51} n_{\text{H}}}. \quad (20)$$

HD is created and destroyed in four exchange reactions involving  $\text{H}_2$  (Table 1),

$$n_{\text{HD}} = \frac{k_{52} n_{\text{D}^+} n_{\text{H}_2} + k_{54} n_{\text{D}} n_{\text{H}_2}}{k_{53} n_{\text{H}^+} + k_{55} n_{\text{H}}}. \quad (21)$$

We note that the rate for collisional destruction of  $\text{H}_2$  by H (rate (8), or R13) used in Enzo is significantly higher than the rate for the same process used by Bromm et al. (2002) for the temperature range  $10^4 \lesssim T \lesssim 10^7$ . The equilibrium abundance of  $\text{H}_2$  at  $T \sim 15000$  K in our calculation is lower by a factor of 6 than that of Johnson & Bromm (2006, see their Figure 1). Simulations of primordial star formation do not reach such high temperatures so this difference is unimportant to the work presented here.

#### REFERENCES

- Abel, T., Anninos, P., Zhang, Y., & Norman, M. L. 1997, *New Astronomy*, 2, 181
- Abel, T., Bryan, G. L., & Norman, M. L. 2000, *ApJ*, 540, 39
- Abel, T., Bryan, G. L., & Norman, M. L. 2002, *Science*, 295, 93
- Abel, T., Wise, J. H., & Bryan, G. L. 2007, *ApJ*, 659, L87
- Anninos, P., Zhang, Y., Abel, T., & Norman, M. L. 1997, *New Astronomy*, 2, 209
- Berger, M. J., & Colella, P. 1989, *Journal of Computational Physics*, 82, 64
- Bromm, V., Coppi, P. S., & Larson, R. B. 2002, *ApJ*, 564, 23
- Bromm, V., & Larson, R. B. 2004, *ARA&A*, 42, 79
- Bryan, G. L., Norman, M. L., Stone, J. M., Cen, R., & Ostriker, J. P. 1995, *Computer Physics Communications*, 89, 149
- Bryan, G. L., & Norman, M. L. 1997, *Computational Astrophysics; 12th Kingston Meeting on Theoretical Astrophysics*, 123, 363
- Bryan, G. L. *Comp. Phys. and Eng.* 1999, 1:2, p.
- Bryan, G. L., & Voit, G. M. 2001, *ApJ*, 556, 590
- Burles, S., & Tytler, D. 1998, *ApJ*, 507, 732
- Ciardi, B., & Ferrara, A. 2005, *Space Science Reviews*, 116, 625
- Colella, P., & Woodward, P. R. 1984, *Journal of Computational Physics*, 54, 174
- Couchman, H. M. P., & Rees, M. J. 1986, *MNRAS*, 221, 53
- Eisenstein, D. J., & Hu, W. 1999, *ApJ*, 511, 5
- Eisenstein, D. J., & Hut, P. 1998, *ApJ*, 498, 137
- Efstathiou, G., Davis, M., White, S. D. M., & Frenk, C. S. 1985, *ApJS*, 57, 241
- Flower, D. R., Le Bourlot, J., Pineau des Forêts, G., & Roueff, E. 2000, *MNRAS*, 314, 753
- Galli, D., & Palla, F. 2002, *Planet. Space Sci.*, 50, 1197
- Galli, D., & Palla, F. 1998, *A&A*, 335, 403
- Gao, L., Yoshida, N., Abel, T., Frenk, C. S., Jenkins, A., & Springel, V. 2007, *MNRAS*, 378, 449
- Glover, S. C. O., & Abel, T. 2008, *ArXiv e-prints*, 803, arXiv:0803.1768
- Glover, S. C., Savin, D. W., & Jappsen, A.-K. 2006, *ApJ*, 640, 553
- Glover, S. C. O., & Jappsen, A.-K. 2007, *ApJ*, 666, 1
- Glover, S. C. O. 2007, *ArXiv e-prints*, 708, arXiv:0708.3086
- Greif, T. H., & Bromm, V. 2006, *MNRAS*, 373, 128
- Haiman, Z., Thoul, A. A., & Loeb, A. 1996, *ApJ*, 464, 523
- Heger, A., Fryer, C. L., Woosley, S. E., Langer, N., & Hartmann, D. H. 2003, *ApJ*, 591, 288
- Johnson, J. L., & Bromm, V. 2006, *MNRAS*, 366, 247
- Kitayama, T., Yoshida, N., Susa, H., & Umemura, M. 2004, *ApJ*, 613, 631
- Komiya, Y., Suda, T., Minaguchi, H., Shigeyama, T., Aoki, W., & Fujimoto, M. Y. 2007, *ApJ*, 658, 367
- Lipovka, A., Núñez-López, R., & Avila-Reese, V. 2005, *MNRAS*, 361, 850
- Machacek, M. E., Bryan, G. L., & Abel, T. 2001, *ApJ*, 548, 509
- Machacek, M. E., Bryan, G. L., & Abel, T. 2003, *MNRAS*, 338, 273
- Machida, M. N., Tomisaka, K., Nakamura, F., & Fujimoto, M. Y. 2005, *ApJ*, 622, 39
- Mackey, J., Bromm, V., & Hernquist, L. 2003, *ApJ*, 586, 1
- McKee, C. F., & Tan, J. C. 2007, *ArXiv e-prints*, 711, arXiv:0711.1377
- Mesinger, A., Bryan, G. L., & Haiman, Z. 2006, *ApJ*, 648, 835
- Nagakura, T., & Omukai, K. 2005, *MNRAS*, 364, 1378
- Omukai, K., & Palla, F. 2003, *ApJ*, 589, 677
- O'Shea, B. W., Bryan, G., Bordner, J., Norman, M. L., Abel, T., Harkness, R., & Kritsuk, A. 2004, *ArXiv Astrophysics e-prints*, astro-ph/0403044
- O'Shea, B. W., McKee, C. F., Heger, A., & Abel, T. 2008, *ArXiv e-prints*, 801, arXiv:0801.2124
- O'Shea, B. W., & Norman, M. L. 2007, *ApJ*, 654, 66
- O'Shea, B. W., Abel, T., Whalen, D., & Norman, M. L. 2005, *ApJ*, 628, L5
- Puy, D., Alecian, G., Le Bourlot, J., Leorat, J., & Pineau Des Forets, G. 1993, *A&A*, 267, 337
- Richter, P., Fang, T., & Bryan, G. L. 2006, *A&A*, 451, 767
- Ripamonti, E. 2007, *MNRAS*, 376, 709
- Romano, D., Tosi, M., Matteucci, F., & Chiappini, C. 2003, *MNRAS*, 346, 295
- Salvatterra, R., Ferrara, A., & Schneider, R. 2004, *New Astronomy*, 10, 113
- Savin, D. W. 2002, *ApJ*, 566, 599
- Shapiro, P. R., & Kang, H. 1987, *ApJ*, 318, 32
- Shu, F. H. 1977, *ApJ*, 214, 488
- Slyz, A. D., Devriendt, J. E. G., Bryan, G., & Silk, J. 2005, *MNRAS*, 356, 737
- Spergel, D. N., et al. 2007, *ApJS*, 170, 377
- Stancil, P. C., Lepp, S., & Dalgarno, A. 1998, *ApJ*, 509, 1
- Tan, J. C., & McKee, C. F. 2004, *ApJ*, 603, 383
- Tegmark, M., Silk, J., Rees, M. J., Blanchard, A., Abel, T., & Palla, F. 1997, *ApJ*, 474, 1
- Truelove, J. K., Klein, R. I., McKee, C. F., Holliman, J. H., II, Howell, L. H., & Greenough, J. A. 1997, *ApJ*, 489, L179
- Tumlinson, J. 2007, *ApJ*, 665, 1361
- Whalen, D., Abel, T., & Norman, M. L. 2004, *ApJ*, 610, 14
- Wise, J. H., & Abel, T. 2007, *ArXiv e-prints*, 710, arXiv:0710.3160
- Yoshida, N., Abel, T., Hernquist, L., & Sugiyama, N. 2003, *ApJ*, 592, 645
- Yoshida, N., Oh, S. P., Kitayama, T., & Hernquist, L. 2007a, *ApJ*, 663, 687
- Yoshida, N., Omukai, K., & Hernquist, L. 2007b, *ApJ*, 667, L117
- Yoshida, N., Omukai, K., Hernquist, L., & Abel, T. 2006, *ApJ*, 652, 6
- Younger, J. D., & Bryan, G. L. 2007, *ApJ*, 666, 647

TABLE 1  
REACTION RATES FOR DEUTERIUM SPECIES

Reaction	Rate Coefficient ( $\text{cm}^3 \text{s}^{-1}$ )	Reference
D1 $\text{D} + e^- \rightarrow \text{D}^+ + 2e^-$	See expression in reference	A97/1 <sup>a</sup>
D2 $\text{D}^+ + e^- \rightarrow \text{D} + \gamma$	See expression in reference	A97/2 <sup>a</sup>
D50 $\text{D} + \text{H}^+ \rightarrow \text{D}^+ + \text{H}$	$2.00 \times 10^{-10} T^{0.402} e^{-37.1/T} - 3.31 \times 10^{-17} T^{1.48}$	GP02/5
D51 $\text{D}^+ + \text{H} \rightarrow \text{D} + \text{H}^+$	$2.06 \times 10^{-10} T^{0.396} e^{-33.0/T} + 2.03 \times 10^{-9} T^{-0.332}$	GP02/6 <sup>b</sup>
D52 $\text{D}^+ + \text{H}_2 \rightarrow \text{H}^+ + \text{HD}$	$10^{-9} \times [0.417 + 0.846 \log T - 0.137(\log T)^2]$	GP02/2
D53 $\text{HD} + \text{H}^+ \rightarrow \text{H}_2 + \text{D}^+$	$1.1 \times 10^{-9} e^{-488/T}$	GP02/4
D54 $\text{D} + \text{H}_2 \rightarrow \text{H} + \text{HD}$	$1.69 \times 10^{-10} e^{(-4680/T+198800/T^2)}$	GP02/1 <sup>c</sup>
D55 $\text{HD} + \text{H} \rightarrow \text{H}_2 + \text{D}$	$5.25 \times 10^{-11} e^{(-4430/T+173900/T^2)}$	GP02/3 <sup>c</sup>

NOTE. — The references are Abel et al. 1997 (A97) and Galli & Palla 2002 (GP02), with the rate numbers used in those papers shown after the reference. The first column gives the rate numbers according to the system used internally within the Enzo code.

<sup>a</sup> The collisional ionization and recombination rates for deuterium are taken from the equivalent rates for hydrogen.

<sup>b</sup> Rate 6 from Galli & Palla 2002 contains a typo and was obtained from the original reference, Savin 2002.

<sup>c</sup> Ripamonti (2007) noted that these rates become unphysically large at  $T \leq 100\text{K}$ , following the example of that paper we set the rates at  $T \leq 100\text{K}$  to be the same as the rate at  $T = 100\text{K}$ .

TABLE 2  
PROPERTIES OF THE SIMULATION HALOS IN THE UNPERTURBED RUNS

Run	$z_{\text{coll}}$	$M_{\text{vir}}$ ( $10^5 M_{\odot}$ )	$R_{\text{vir}}$ (pc)	$T_{\text{vir}}$ (K)	$T_{\text{min}}$ (K)	$n(T_{\text{min}})$ ( $10^3 \text{cm}^{-3}$ )
Halo1-H2	14.55	10.84	213.0	1610	268	5.5
Halo1-HD	14.71	10.24	207.0	1566	286	4.1
Halo2-H2	15.35	9.62	194.7	1563	322	3.6
Halo2-HD	15.34	9.82	196.2	1585	300	3.2
Halo3-H2	14.88	6.72	177.9	1195	290	31.6
Halo3-HD	14.74	6.94	181.5	1211	66	23.7
Halo4-H2	14.56	9.37	202.9	1462	268	5.0
Halo4-HD	15.02	7.93	186.4	1347	103	85.2

NOTE. — The runs are labeled “H2” to indicate a run without deuterium chemistry and “HD” when deuterium is included; they are otherwise identical. The redshift of collapse is determined as the redshift when the central density exceeds  $10^{10} \text{cm}^{-3}$ ; the virial mass, radius, and temperature are calculated at this time as well. The minimum temperature  $T_{\text{min}}$  is calculated at the final timestep and found by fitting a cubic polynomial to the  $n - T$  plane in logarithmic space, in the region around the temperature minimum (e.g., the upper panel of Figure 5). The value of  $T_{\text{min}}$  and corresponding density  $n(T_{\text{min}})$  are determined from the minimum of the fitting function, and illustrate the effect of HD cooling in the region of lowest temperature.

TABLE 3  
PROPERTIES OF THE SIMULATION HALOS IN THE IONIZED RUNS

Run	$z_{\text{coll}}$	$M_{\text{vir}}$ ( $10^5 M_{\odot}$ )	$R_{\text{vir}}$ (pc)	$T_{\text{vir}}$ (K)	$T_{\text{min}}$ (K)	$n(T_{\text{min}})$ ( $10^3 \text{cm}^{-3}$ )
Halo1-H2	13.53	12.72	240.5	1673	132	1.3
Halo1-HD	15.06	7.38	181.5	1286	55	9.1
Halo2-H2	18.22	2.21	101.5	690	132	2.2
Halo2-HD	18.74	1.93	94.4	647	61	12.5
Halo3-H2	17.05	2.29	109.3	662	132	2.1
Halo3-HD	15.37	4.57	151.8	953	58	9.4

NOTE. — See Table 2 for a description of the table format.